Numerical Study of FIO of Circular Cylinder with Different Heights of Passive Turbulence Control Strips

Chunhui Ma and Decheng Wan*

State Key Laboratory of Ocean Engineering, School of Naval Architecture, Ocean and Civil Engineering, Shanghai Jiao Tong University, Collaborative Innovation Center for Advanced Ship and Deep-Sea Exploration, Shanghai 200240, China

*Corresponding author: dcwan@sjtu.edu.cn

Abstract

Vortex-induced vibrations (VIV) and galloping are commonly referred to as fluid induced oscillation(FIO). For a spring-mounted rigid cylinder inflow, an isolated smooth circular cylinder could only undergo VIV but not gallop. However, non-circular sections or circular sections with attachments could be subjected to large amplitude galloping oscillations. In this paper, two-dimensional RANS equations with SST k – ω turbulence model are used to simulate the flow induced oscillation of seven single circular cylinders (P0, P1, P1.4, P2, P3, P5, P10) with different height PTC (Passive Turbulence Control) strips and supported by spring stiffness in steady uniform flow. The simulation is carried out by the in-house CFD solver naoe-FOAM-SJTU, based on the open source toolbox OpenFOAM. The oscillation response of P0 to P10 at $Re = 3.71 \times 10^4$ and $Re = 1.03 \times 10^5$ are being presented and analyzed. The amplitude ratio and frequency ratio has different trends following the height of the PTC changes. However, vibration responses of P10 are very similar regardless of the Reynolds number. Moreover, KC number as an important parameter of vortex regime in FIO, vortex structures are analyzed using vorticity images from the CFD result. Single vortex shedding structures are found in the wake as $KC < 1.8$. 3P+S vortex shedding appears when $KC > 4$.

Keywords: VIV; galloping; naoe-FOAM-SJTU solver; RANS; passive turbulence control

1 Introduction

Vortex-induced vibrations (VIV) and galloping are the two common fluid-structure interaction phenomenon which can be observed in crossflow. They are commonly referred to as fluid induced oscillation(FIO). The excitation of the VIV is caused by the alternating shedding of eddy current from each side of the cylinder. Also, time-varying forces at the frequency of vortex shedding give rise to periodic changes in the pressure distribution on the body surface. For a spring-mounted rigid cylinder, an isolated smooth circular cylinder could only undergo VIV does not gallop. However, such as triangle, square non-circular sections could be subjected to large amplitude galloping oscillations (Parkinson and Sullivan, 1979; Bokaian and Geoola, 1984b) [1][2]. And circular sections with like splitter plate attachments also could experience galloping (Nakamura et al., 1994) [3]. Furthermore, the proximity of another cylinder would also induce galloping excitation in circular cylinders (Bokaian and Geoola, 1984a) [4]. Therefore, the phenomenon of galloping is not due to the normal vortex shedding, which is an instability phenomenon caused by the motion of the shear layers on both sides of the cylinder.

Some scholars applied straight rough strips (PTC, passive turbulence control) to the surface of the cylinder to change the geometry section (Chang et al., 2010; Chang et al., 2011; Park et al., 2011) [5-7]. Width, roughness, and circumferential location on the cylinder are the parameters tested experimentally in the Water Channel located in the Marine Renewable Energy Laboratory (MRELab) of the University of Michigan. Also, many scholars are devoted to

studying the motion mechanism of passive turbulence control system and applying them to new energy fields. (Bernitsas et al., 2009; Lee et al., 2011, Sun et al.,2017; Sun et al., 2019) [8-11]

However, the replacement of different PTC strip in most experiments is very time consuming and requires recalibration, while the CFD method makes this efficient. Meanwhile, CFD make the local vortex shedding visualization, so this is easier to analyze the mechanism of FIO. In this study, two-dimensional RANS equations with SST k – ω turbulence model are used to simulate the flow induced oscillation of seven single circular cylinders (P0, P1, P1.4, P2, P3, P5, P10) with different height PTC (Passive Turbulence Control) strips and supported by spring stiffness in steady uniform flow at $Re = 3.71 \times 10^4$ and $Re = 1.03 \times 10^5$ 103000 (primarily the TrSL3 flow regime (Zdravkovich, 1997) [12]). The simulation is carried out through the CFD solver naoe-FOAM-SJTU developed by the open source toolbox OpenFOAM. The objective is to understand the impact of PTC on flow induced oscillation by changing the height of strips attached on the cylinder, and analyze vortex structures using high-resolution imaging from the CFD result. This paper first introduces the numerical methods used in naoe-Foam-SJTU solver, including turbulence simulation method, dynamic overset grid technique and spring system in section 2. Section 3 illustrates computational physical model, geometric parameters, computational domain, grid and boundary conditions. Then in section 4, the free decay of the spring system is verified, the amplitude and frequency response of seven cylinders are conduct under two Reynolds numbers to evaluate the effect of the height of PTC on the FIO. Also, vortex structures are analyzed from the CFD result. Finally, section 5 concludes this paper.

2 Mathematical model and numerical method

All numerical simulations in this study are based on the in-house 6DoF CFD solver naoe-FOAM-SJTU (Shen and Wan, 2015) [13], which was developed on the open-source CFD software OpenFOAM. And the dynamic overset grid technology was implemented into the solver in coupled with Suggar ++(Noack, 2005, Noack et al., 2009) [14,15] to facilitate large amplitude hull motions. The naoe-FOAM-SJTU has been validated via a majority of marine and ocean engineering problems. (Cao and Wan, 2010; Zhou et al., 2013; Wang et al., 2017) [16-18].

2.1 Governing equations and turbulence modeling

The turbulent flow is a highly complex three-dimensional unsteady, irregular flow with rotation. The simulations for turbulence are currently divided into direct numerical simulation (DNS), large eddy simulation (LES), and the use of Reynolds average NS equation simulation (RANS). Because DNS and LES have high requirements on a computing resource, so its applicability to engineering problems needs to be improved. RANS equation is adopted in this study. The Reynolds average NS equation is as follows:

$$\frac{\partial u_i}{\partial x_i} = 0 \tag{1}$$

$$\frac{\partial}{\partial t}(\rho u_i) + \frac{\partial}{\partial x_j}\left(\rho u_i u_j\right) = \frac{\partial p}{\partial x_j} + \frac{\partial}{\partial x_j}(2\mu S_{ij} - \rho\overline{u_j' u_i'}) \tag{2}$$

In order to solve the equations, a turbulence model is introduced to determine the Reynolds stress term $-\rho\overline{u_j' u_i'}$. The currently used turbulence models are k − ε and k − ω models. This paper uses the SSTk − ω model, which combines the advantages of the above two types of

models to ensure the accuracy and reliability of the solution near the wall, and can better solve the flow problem with negative pressure gradient. Specifically, the problems discussed in this paper require the capture of flow separation and wake near-field detailing. The corresponding mesh should satisfy the near-walled body-fitted grid placed within the viscous bottom layer and the mesh near the wall is dense. The SST k − ω model can better meet the above requirements. The equation for the SST k − ω model in the OpenFOAM solver is referred to Menter,1994. [19]

2.2 Overset Grid

In this paper, the overset grid program Suggar++ is used to calculate Domain Connectivity Information (DCI). The information mainly includes unit information (hole unit, interpolation unit, contribution unit, orphan unit) and interpolation weight coefficient. The solver implements fully parallelized flow field solving and overset mesh burrow interpolation calculations by running OpenFOAM and Suggar++ in different processes. Grid motion and DCI information exchange between different processes are implemented through the Message Passing Interface (MPI).

2.3 Spring system

The spring system is an important factor in studying the FIO response of a rigid cylinder with elastic support. The spring system in the experiment called Vck (Virtual spring-damping device) can realize the oscillator of the real spring by changing the parameters such as system stiffness and damping (Sun, 2015) [20]. Also, the mooring system of naoe-FOAM-SJTU is adopted to simulate the spring and more convenient to adjust the parameters (Zhao et al., 2018) [21]. Currently the mooring system supports four types of mooring line, which include linear spring, catenary, PEM (piecewise extrapolation method) and LMM (lumped mass method). Moreover, it is convenient to extend more complex mooring system and update new mooring line types based on the current framework. In the present study, all mooring lines are treated as linear springs.

3 Physical model and simulation design

3.1 Physical model

The physical model is referred to MRELab of University of Michigan (Chang, 2011; Bernitsas, 2009) [6][8]. A simple schematic of the circular cylinder oscillation system in the present work is shown in Figure 1. The elements of this oscillator include a rigid circular cylinder of diameter *D*, length *L*, stiffness *K*, and system damping *C*. The cylinder is limited to oscillating in one direction, that is, perpendicular to the direction of incoming flow.

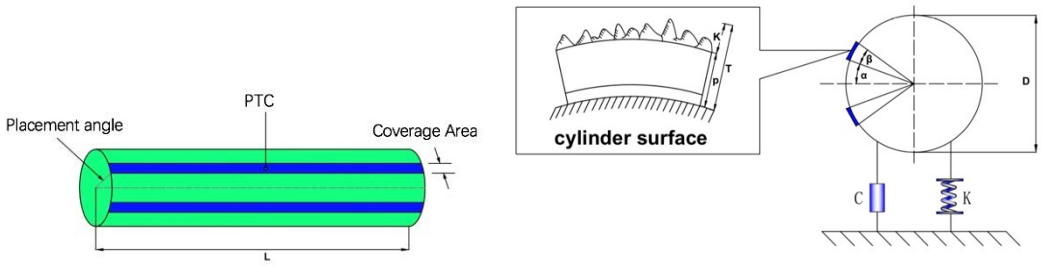

Figure 1. Physical model

PTC strips acts like ‘step’ are attached to the smooth cylinder, the total thickness (*T*) of PTC strips is defined as *T*=*k*+*P*, where *k* is the roughness height and p is the paper thickness.

Meanwhile α is the strip placement angle and value of β indicates coverage area. The parameters for this system are listed in table 1. The roughness act as a 'catalyst' to promote galloping fully-developed in the experiment (Chang, 2010)[5], but it does not significantly influence the oscillation response, so the wall function with roughness temporarily not be considered in this paper, which means k in all case should be set as zero. Table 2 shows 7 cases (P0, P1, P1.4, P2, P3, P5, and P10), which are the circular cylinder of the same diameter with various height T, by changing the parameter p. It should be noted that P0 is a smooth cylinder without PTC strip, 0.847mm is setting as P1's strip height references the experiment (Sun,2016) [20], and P1.4 to P10 respectively set the PTC height to 1.4 times to 10 times this value.

Table 1. Parameters of the oscillatory system

Parameters	Symbol(unit)	Dimension
Diameter	D [m]	0.0889
Length	L [m]	0.894
strip placement angle	α[°]	20
strip coverage angle	β[°]	16
Spring stiffness	k [N/m]	600
Damping ratio	ζ	0.02
Mass	m [kg]	7.286
Mass ratio	m^*	1.343
Natural frequency in air	$f_{n,air}$ [Hz]	1.44
Natural frequency in water	$f_{n,water}$ [Hz]	1.09

Table 2. Different height of PTC

	P0	P1	P1.4	P2	P3	P5	P10
T(mm)	0	0.847	1.198	1.694	2.541	4.235	8.47

3.2 Computational Domain and Grid Generation

Figure 3(a) shows the computational domain for all simulations in this study, which size is 20D*32D, D is the diameter of the cylinder. The center of gravity of the oscillating system is located 8D downstream of the inlet boundary condition along the longitudinal centerline of the domain. The boundary condition for velocity is set as U at inlet and zero gradient at outlet. A zero gradient boundary condition is specified for both inlet and outlet for pressure and the value is zero. The boundary condition of front and back lateral are set as empty for this case is a two-dimension simulation. The top and bottom conditions are considered as far-field boundary. For the surface of PTC as moving wall, nutUSpaldingWallFunction is a wall function that can solve any of the conditions of the near wall surface including the buffer layer, so it is selected as a wall function of moving wall.

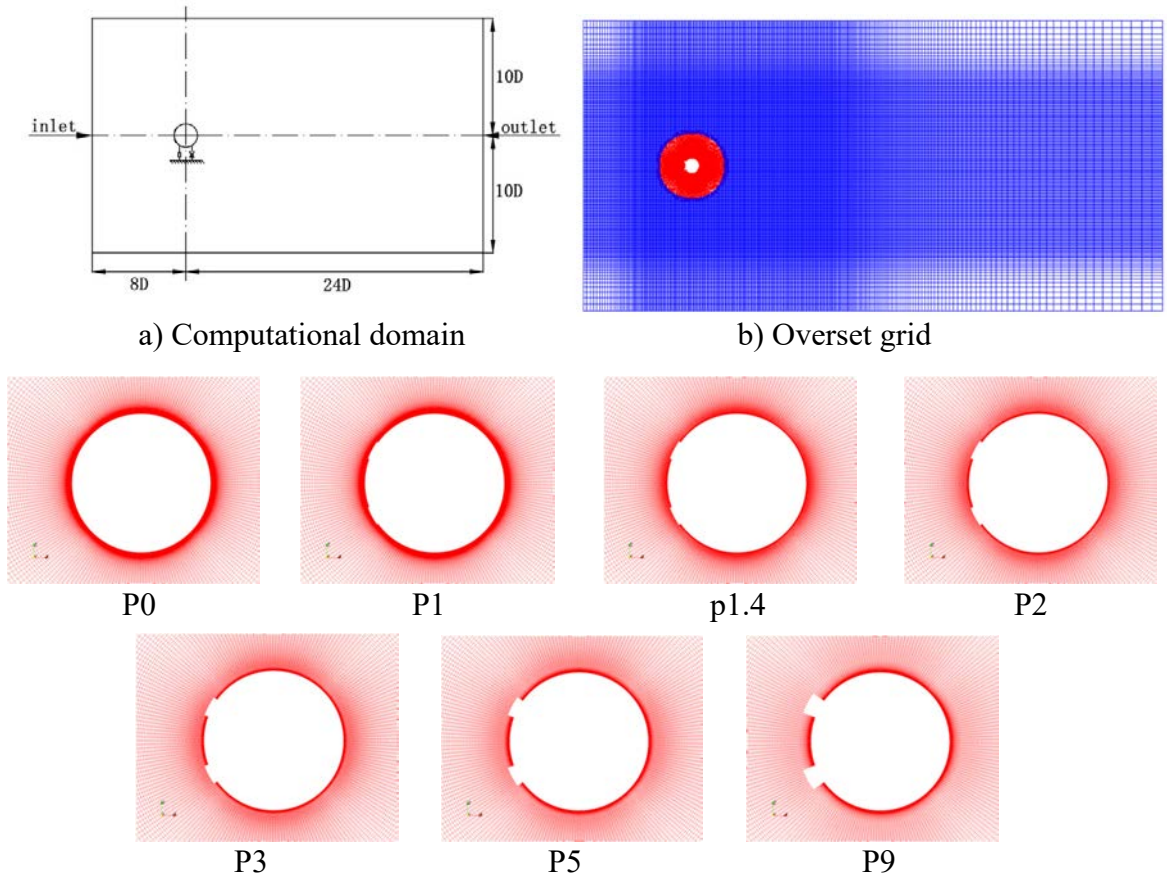

a) Computational domain b) Overset grid

c) close-up grid of P0 to p10

Figure 2. Computational domain and grid

The overset grid technique has been verified as a reliable grid application in a fixed circular flow numerical simulation within a vast Reynold number ($6.31 \times 10^4 \sim 7.57 \times 10^5$) (Ye et al, 2018) [22], which can achieve better numerical results than dynamic grid techniques. So an overset grid system is used throughout the present study to simulate the FIO response of cylinders. The overset grid system Contains two sets of independent grids, as shown in Figure 2(b), the blue grid is the background and the red part is hull grid, which are generated separately using the Pointwise grid-generating software. Then background and hull grids are merged into one set of grid in naoe-Foam-SJTU solver. The two mesh-blocks do not share any points, edges or faces. Flow information are exchanged by interpolation using domain connectivity information (DCI) generated by Suggar++. Figure 2(c) shows a close-up of a cylindrical grid of seven different PTC heights. For all P0 to P10 cases, the dimensionless wall spacing of the first layer close to the wall mesh satisfies y + <5, which makes sure the first layer cells are located in the viscous sublayer although nutUSpaldingWallFunction is applied. The total cell number is around 80,000 to 86,000. Also, the PIMPLE (merged PISO-SIMPLE) algorithm is used to solve the coupled pressure and velocity. PIMPLE treats every single time step as steady-state and performs SIMPLE correctors outside the PISO loop. It can run robustly at larger time step where Courant number is larger than one.

4 Results and discussion

4.1 Free decay

For validate spring stiffness, free decay tests are carried out. The free decay test allows the object to oscillate according to a specified initial offset or speed without inflow. The spring system in noae-FOAM-SJTU only works effectively in the tension state, so symmetrical spring with pre-tension force is arranged along the direction of the vibration of the cylinder. The stiffness and pre-tension are adjusted to ensure that the system is always effective and accurate. The effective stiffness must be consistent with the experiment. Linear spring system test parameters refer to experimental data (sun et al, 2015) [23]. That is, mass of cylinder is 5.4878kg, mass ratio $m^* = \frac{m_{osc}}{m_{dis}} = 1.012$, m_{dis} is the displacement mass of water when cylinder is merged in the channel. Spring stiffness is set to *600N/m*, damping coefficient is 0.0453, pre-tension is given 210N to ensure that the linear spring system is always tensioned as long as the amplitude of cylinder is less than 4. The parameters and results of free decay test is shown in Table 3, while Figure 5 presents the time history curve and spectrum analysis of the free decay test. The spring system and experimental error are less than 1.373%, indicating that the current spring system provides the correct effective stiffness.

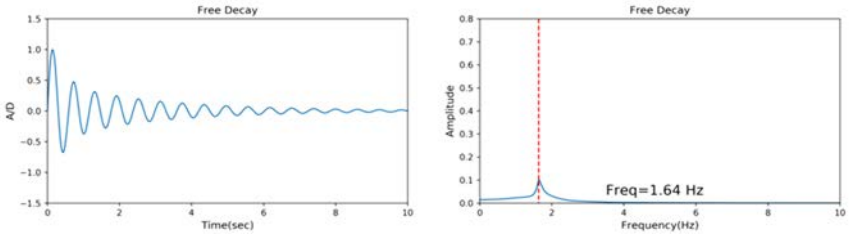

Figure 3. Time history and spectrum of free decay

Table 3. Free decay parameters

k[N/m]	Damping ratio	c(Ns/m)	m(kg)	m*	T_{exp}	T_{cfd}	Dev.
600	0.0453	5.204	5.4878	1.012	0.6015	0.6098	0.01373

4.2 Amplitude response

The amplitude of the cylinder is one of the critical properties which can adequately describe and quantify FIO. The amplitude ratios A/D of seven cases (P0 to P10) are plotted in Figure 4 at $Re = 3.71 \times 10^4$ and $Re = 1.03 \times 10^5$. The corresponding time history is also marked in the figure. The experimental values of P1 and the data of seven present numerical case are listed in Table 4. At $Re = 3.71 \times 10^4$, the amplitude ratio of P1 in the experiment is 0.352, and the value of P1 of the present study is 0.276, which is 20% smaller than experimental data. Since this is a complex flow separation of high Reynolds number, it can still be considered that the current numerical calculations and experiments consistently achieve the initial branch of VIV, even with a 20% error. Then, the amplitude ratio of the cylinders with P0 to P10 can be compared and analyzed. As can be seen from the figure4 (a), while the height of PTC increases from zero, A/D increase slightly at first, then slowly bend down at P1.4 heights. Till the height of PTC up to P3, the amplitude reaches the lowest point, after that, it tends to a steady rise again. When the PTC height is up to the highest of this group study, amplitude ratio is also up to the maximum. At $Re = 1.03 \times 10^5$, that should be a large amplitude galloping region as depicted in experimental data. However, galloping phenomenon has not appeared in any present

numerical simulation cases. As can be seen from Figure 4(b), the range A/D keep decreasing constantly from P0 to P10, except a slight increase at P2. So the higher the PTC, the more obvious the amplitude decline trend. It is revealed here that the increase in the height of the PTC possibly causes the vibration to be suppressed at $Re = 1.03 \times 10^5$.

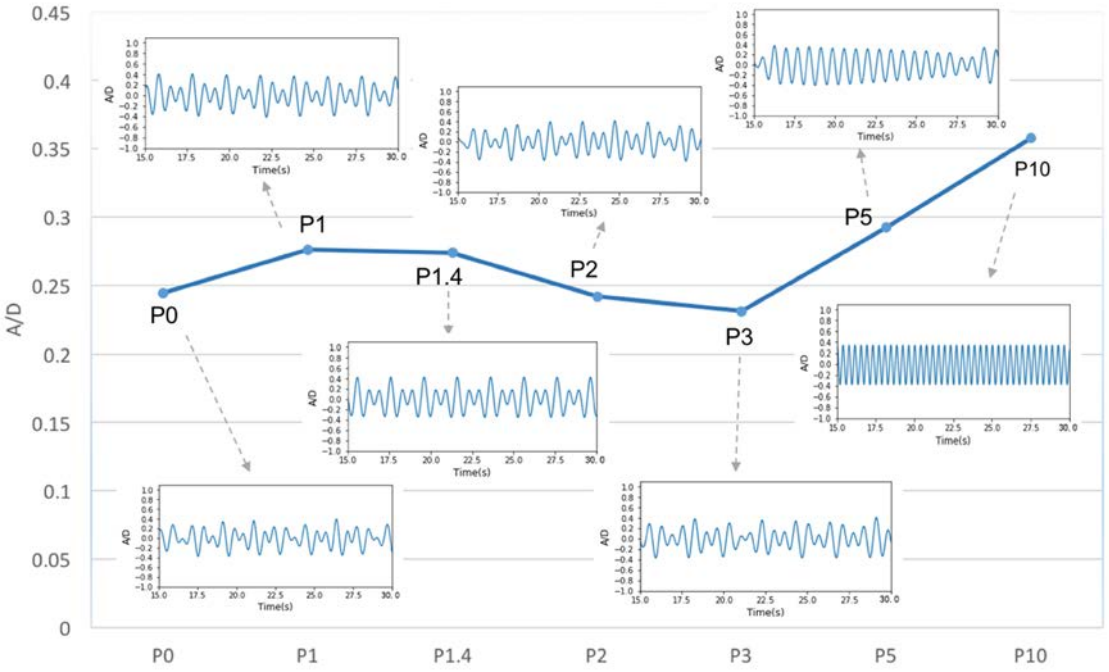

a) $Re = 3.71 \times 10^4$

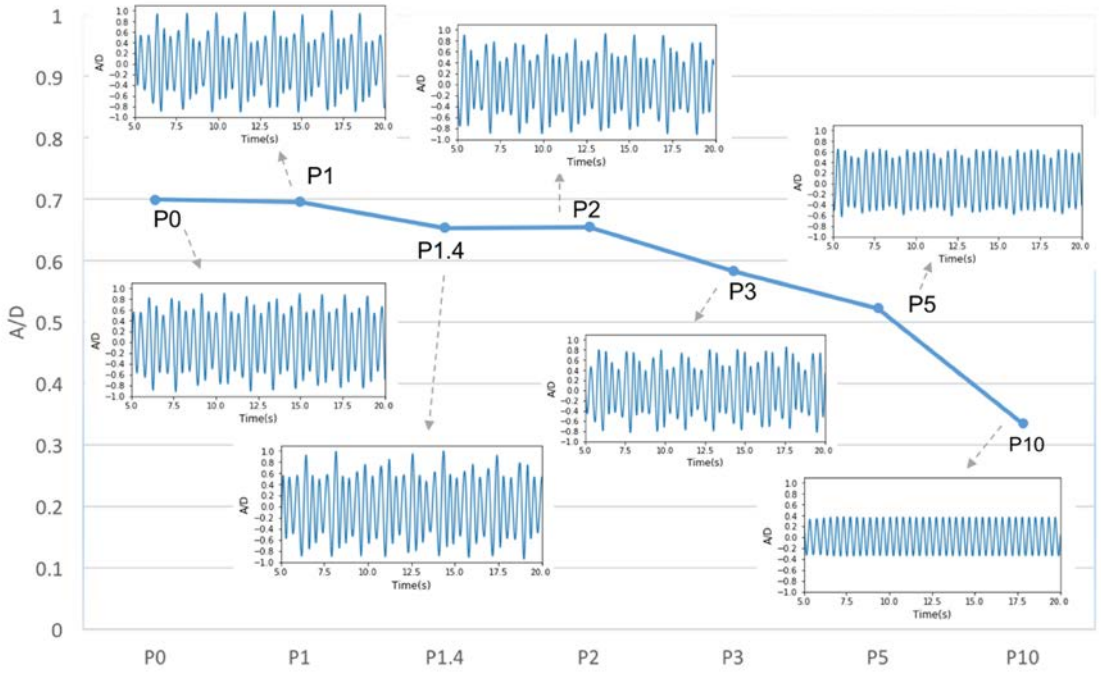

b) $Re = 1.03 \times 10^5$

Figure 4. Amplitude ratio and displacement history

Table 4. Amplitude ratio

	Re	$P1_{exp}$	P0	P1	P1.4	P2	P3	P5	P10
A/D	3.71×10^4	0.352	0.244	0.276	0.274	0.242	0.231	0.292	0.358
	1.03×10^5	1.662	0.699	0.696	0.653	0.655	0.583	0.522	0.335

4.3 Frequency response

The oscillation frequency results are shown in Figure 5. Where the frequency ratio $f^* = f_{osc}/f_{n,air}$ of the cylinder is plotted vs. Reynolds. The oscillation frequency f_{osc} is calculated by FFT (Fast Fourier Transform) of the time history of the cylinder over the recorded period. At $Re = 3.71 \times 10^4$, the frequency ratio is around 1 and from P0 to P5, which assumes a practically constant value, which looks like not be affected significantly by the height of the PTC except P10. From P5 to P10 height, there is a sharp increase, the change at this time is the same as the amplitude ratio. At $Re = 1.03 \times 10^5$, all cases have a very high frequency (Table 5, and Fig.5b). The data of frequency ratio appears a slow upward trend. According to the experimental result (Sun et al. 2016)[20], at the Reynolds number is higher than 10^5, there should be low frequency and high amplitude galloping by changing the height of passive turbulence control. However, the numerical results show that the oscillation still maintains high-frequency oscillation and does not reach the instability of galloping.

Table 5. Frequency ratio

	Re	$P1_{exp}$	P0	P1	P1.4	P2	P3	P5	P10
f*	3.71×10^4	0.649	1.054	1.043	1.032	1.032	1.021	0.982	1.794
	1.03×10^5	0.846	1.567	1.567	1.604	1.613	1.604	1.663	1.792

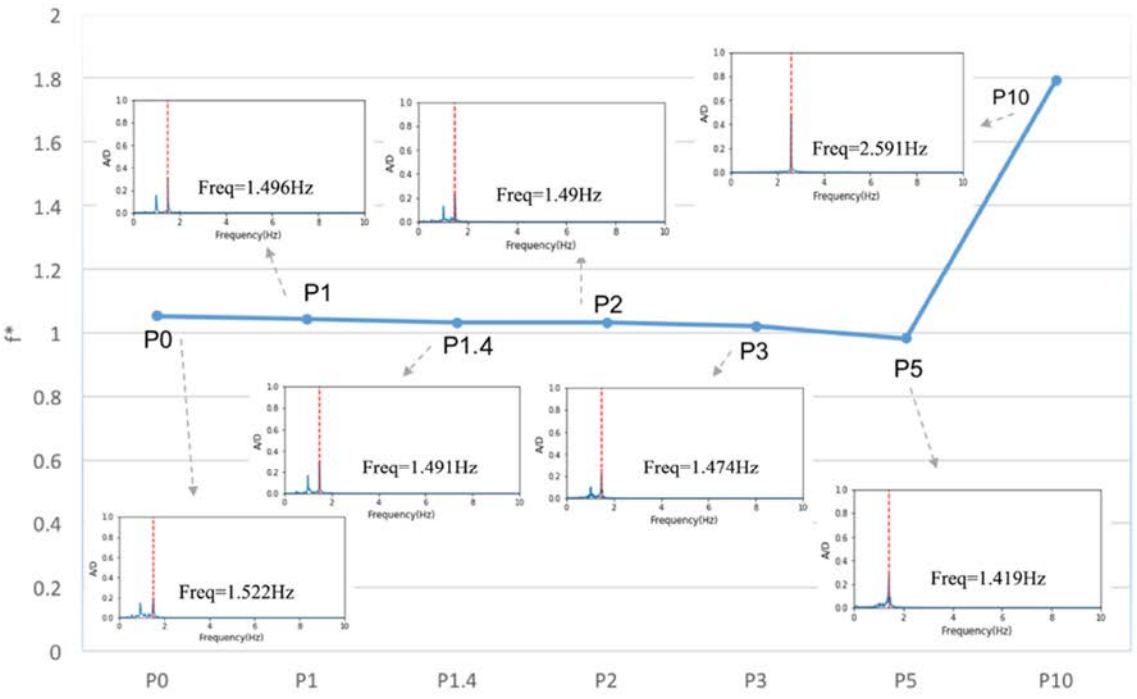

a) $Re = 3.71 \times 10^4$

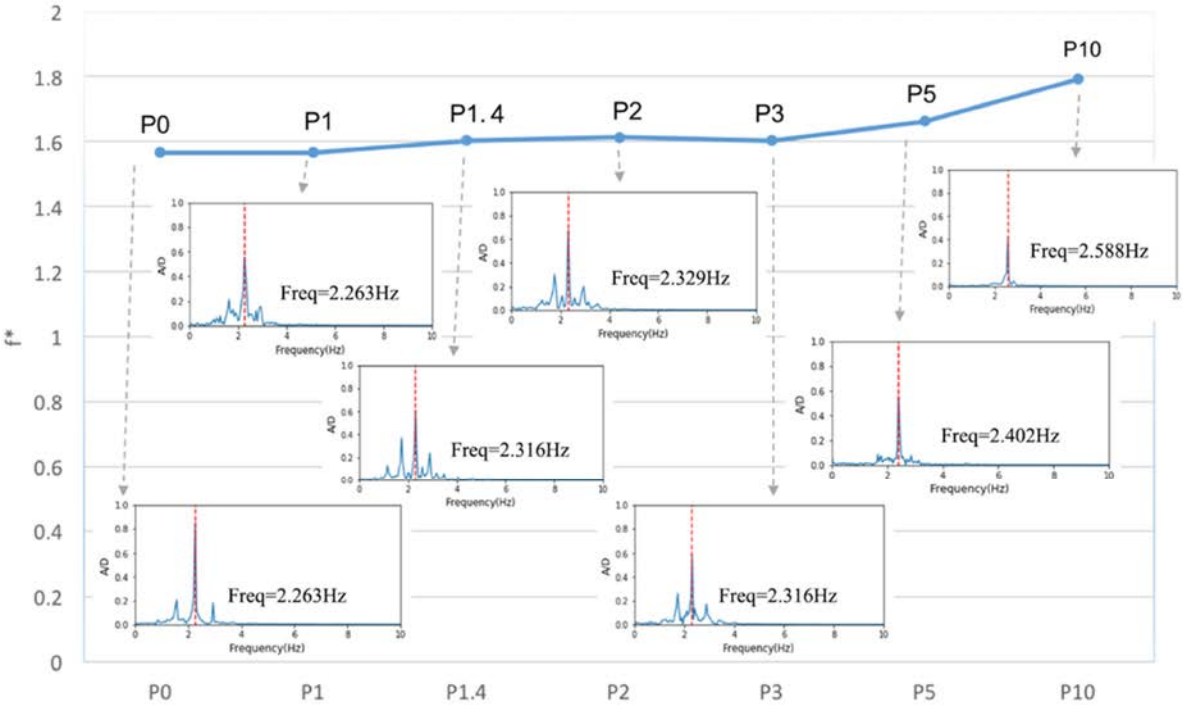

b) $Re = 1.03 \times 10^5$

Figure 5. Frequency ratio and spectral analysis

4.4 Vortex shedding

The vortex shedding works have been considerable light on the understanding of the complex behavior of vortex motion in various regime. Williamson (1985) has described the vortex trajectory patterns in quite a systematic manner [24]. And KC number is an important parameter of vortex regime in FIO, the physical meaning can probably be best explained by reference to Equation 3, where A is the amplitude of the motion.

$$KC = \frac{2\pi A}{D} \tag{3}$$

Table 6. KC number

	Re	P0	P1	P1.4	P2	P3	P5	P10
KC	3.71×10^4	1.535	1.735	1.720	1.519	1.452	1.837	2.247
	1.03×10^5	4.394	4.372	4.105	4.114	3.665	3.284	2.103

Low KC number therefore means that the orbital motion of the water particles is small relative to the total width of the cylinder D. When KC number is tiny, separation behind the cylinder may not even occur. On the other hand, large KC numbers mean that the water particle travels quite vast distances relative to the diameter of cylinder D, resulting in separation and probably vortex shedding (Sarpkaya (1986) and Honji (1981)) [25,26], most of their study concentrated their attention on the KC number dependence or low Re number less than 10^4. As the Reynolds number is less than 10^3, $KC < 1.1$ is laminar flow around the cylinder. Vortex shedding appears when $KC > 7$. Moreover, vortex regime can be divided $7 < KC < 15$ (single pair), $15 < KC < 24$ (double pair), $24 < KC < 32$ (three pair), $32 < KC < 40$ (four pair), etc.

However, for higher Reynolds numbers, the relationship between kc and regime is not clearly defined. In this study, the Reynolds number exceeded 10^5, and the KC values for several cases are given in Table 5, according to the range of kc and the analysis of amplitude and frequency, since the vibration is similar, the vortex diagrams of P1, P5 and P10 under two Reynolds are given here. At $Re = 3.71 \times 10^4$, when $KC < 1.8$, only S (single vortex) shedding appears. When $KC > 1.8$, a slight pair vortex shedding can be found in Figure (b). In the case of P10, an asymmetrical vortex appears on both sides of the cylinder. From the figure, it can be seen that both P (pair vortex) and S appear simultaneously. At $Re = 1.03 \times 10^5$, when $KC > 4$ (P0, P1, P1.4, P2), vortex shedding is 3P+S, when $KC = 3.284$ and $KC = 2.103$, pair vortex and single vortex are alternately appearing regularly. Vortex shedding is suppressed and tend to single pair vortex shedding at P10.

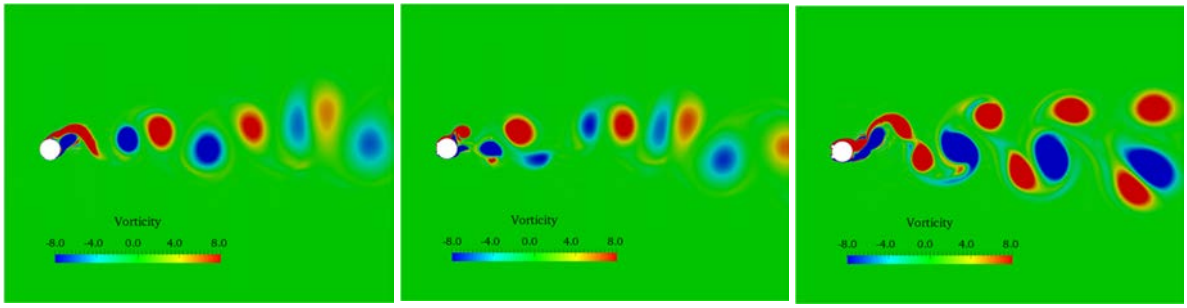

a) P1 b) P3 c)P10

Figure 6. Vortex pattern at $Re = 3.71 \times 10^4$

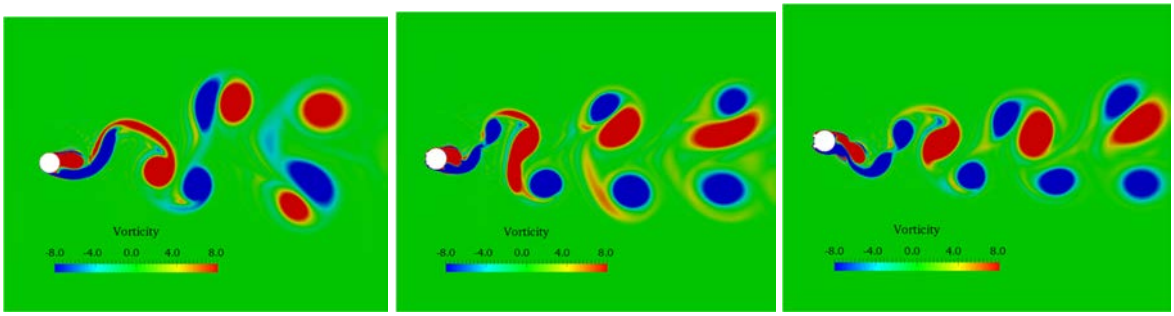

a) P1 b) P3 c)P10

Figure 7. Vortex pattern at $Re = 1.03 \times 10^5$

4.5 Comparison in different flow region

The amplitude and frequency response of $Re = 3.71 \times 10^4$ and $Re = 3.71 \times 10^4$ are put together for comparative analysis. As can be seen from the figure 8(a), under different Reynolds numbers, the amplitude ratio of P0, P1, P1.4, P2, P3 under higher Reynolds number is about twice times compared with lower Reynolds number. As the height increases, the amplitude difference between the same cylinders becomes smaller and smaller in the case of two Reynolds numbers. There is almost no difference in the amplitude of P10, which can be seen from the amplitude displacement history of Figure 4(a)(b). The frequency ratio at $Re = 3.71 \times 10^4$ *and* $Re = 1.03 \times 10^5$, as shown in Figure 8(b). Similarly, the frequency is the same at P10 case, regardless of the Reynolds number. It can be seen from the time history curve that the vibration of p10 is very stable, and the consistency also is conducted from their analysis of the vortex pattern. The vortex structure of Figures 6 and Figures 7 also illustrates the

consistency of the P10 oscillation.

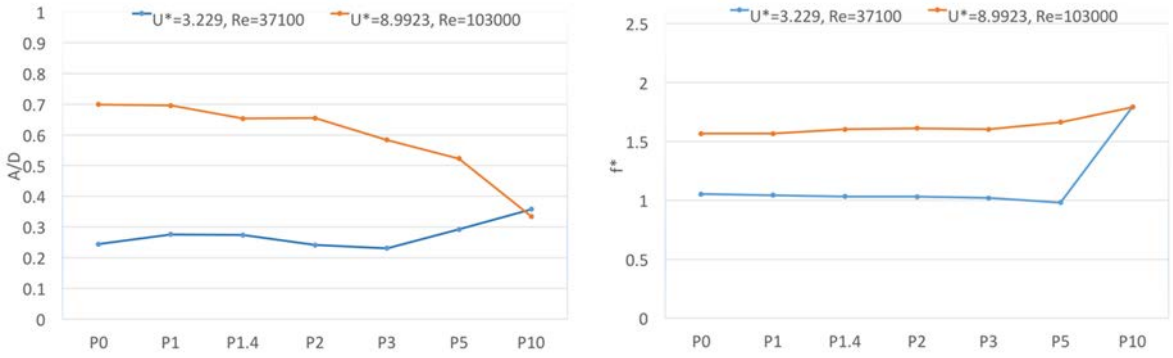

a) Amplitude ratio b) Frequency ratio

Figure 8 Amplitude ratio and frequency ratio of P10

5 Conclusion

The Flow Induced Oscillation of a single, rigid, circular cylinder on linear spring with different height passive turbulence control (PTC) strips were investigated using Reynolds-Averaged Naiver-Stokes equations with $SSTk-\omega$ model at $Re = 3.71 \times 10^4$ and $Re = 1.03 \times 10^5$. All numerical simulations in this study are based on the in-house 6DoF CFD solver naoe-FOAM-SJTU, which developed by open source toolbox OpenFOAM. The following conclusions can be drawn.

(1) At $\mathrm{Re} = 3.71 \times 10^4$, the amplitude ratio and frequency ratio of P1 can realize the initial branch of VIV compared with experimental data. With the height increase of the PTC strips, oscillation amplitude first increases slowly and then show a downward trend, but rise again at p5 and p10. Moreover, oscillation frequency responds almost keep stable from P0 to P5, only with suddenly high-frequency oscillation at P10 case.

(2) At $\mathrm{Re} = 1.03 \times 10^5$, the amplitude ratio decreases as the PTC height increases. The value of amplitude at P10 is almost half of the value of P0, which illustrates PTC can suppress the oscillation in this Reynold number. At the same time, the frequency response at this Reynolds number is gradually increasing.

(3) KC numbers are introduced to analyze wake vortex shedding. Single vortex appears as $\mathrm{KC} < 1.8$. Vortex shedding is 3P+S pattern as $\mathrm{KC} > 4$. When $\mathrm{KC} = 3.284$ and $\mathrm{KC} = 2.103$, pair vortex and single vortex are alternately appearing regularly at $\mathrm{Re} = 1.03 \times 10^5$.

(4) The existence of PTC is similar to a “step”, which determines the flow separation point of the incoming stream. However, the galloping with large amplitude and lower frequency phenomenon does not found in the CFD simulation. The reason may be the FIO at high Reynolds number involves strong flow separations and RANS is not appropriate to employ for it employs statistical averaging procedure to model the mean flow quantities the turbulent fluctuations are eliminated during averaging.

The above study is the beginning of research on passive turbulence control in the flow around a cylinder. The purpose is to better analyze the oscillation response of VIV and galloping by parameter adjustment, to study how to suppress or stimulate FIO. Next, delayed DES (DDES) based on the two-equation shear stress transport (SST) model would be applied in the FIO turbulence modeling and the roughness wall function will be studied in depth.

Acknowledgement

This work is supported by the National Natural Science Foundation of China (51879159,

51490675, 11432009, 51579145), Chang Jiang Scholars Program (T2014099), Shanghai Excellent Academic Leaders Program (17XD1402300), Program for Professor of Special Appointment (Eastern Scholar) at Shanghai Institutions of Higher Learning (2013022), Innovative Special Project of Numerical Tank of Ministry of Industry and Information Technology of China (2016-23/09) and Lloyd's Register Foundation for doctoral student, to which the authors are most grateful.

References

[1] Parkinson, G.V., Sullivan, P.P., 1979. Galloping response of towers. J. Ind. Aerodyn. 4, 253–260.
[2] Bokaian, A.R., Geoola, F., 1984b. Hydroelastic instabilities of square cylinders. J. Sound Vib. 92, 117–141.
[3] Nakamura, Y., Hirata, K., Kashima, K., 1994. Galloping of a circular cylinder in the presence of a splitter plate. J. Fluids. Struct. 8, 355–365.
[4] Bokaian, A., Geoola, F., 1984a. Wake-induced galloping of two interfering circular cylinders. J. Fluid. Mech. 146, 383–415.
[5] Chang, C.C., 2010. Hydrokinetic Energy Harnessing by Enhancement of Flow Induced Motion using Passive Turbulence Control, Naval Architecture and Marine Engineering. University of Michigan, Ann Arbor, MI, USA (Ph.D. Dissertation).
[6] Chang, C.C., Kumar, R.A., Bernitsas, M.M., 2011. VIV and galloping of single circular cylinder with surface roughness at $3 \times 10^4 \leq \mathrm{Re} \leq 1.2 \times 10^5$Ocean Engineering 2011(38), 1713–1732.
[7] Park, H., Kumar, R.A., Bernitsas, M.M., 2013. Enhancement of flow-induced motion of rigid circular cylinder on springs by localized surface roughness at $3 \times 10^4 \leq \mathrm{Re} \leq 1.2 \times 10^5$.Ocean Engineering 2011(72),403–415.
[8] M.M. Bernitsas, K. Raghavan, Converter of Current, Tide, or Wave Energy, United States Patent and Trademark Office, Patent# 7,493,759 B2 issued on February 24, 2009.
[9] J.H. Lee, M.M. Bernitsas, High-damping, high-Reynolds VIV tests for energy harnessing using the VIVACE converter, J. Ocean Eng. 38 (16) (2011) 1697e1712.
[10] Sun, H., Ma, C., Kim, E. S., Nowakowski, G., Mauer, E., & Bernitsas, M. M. (2017). Hydrokinetic energy conversion by two rough tandem-cylinders in flow induced motions: Effect of spacing and stiffness. Renewable Energy, 107, 61-80.
[11] Sun, H., Bernitsas M. M. (2019) Bio-Inspired Adaptive Damping in Hydrokinetic Energy Harnessing using Flow-Induced Oscillations. Energy,
[12] Zdravkovich, M.M., 1997. Flow Around Circular Cylinders, Volume 1: Fundamentals. Oxford University Press, England.
[13] Shen, Z., Wan, D., Carrica, P.M., 2015. Dynamic overset grids in OpenFOAM with application to KCS self-propulsion and maneuvering. Ocean Eng. 108, 287–306.
[14] Noack, R.W., 2005. SUGGAR: a general capability for moving body overset grid assembly. In: Proceedings of the 17th AIAA Computational Fluid Dynamics Conference. Toronto, Ontario, Canada, AIAA 2005–5117.
[15] Noack, R.W., Boger, D.A., Kunz, R.F., Carrica, P.M., 2009. Suggar++: an improved general overset grid assembly capability. In: Proceedings of the 19th AIAA Computational Fluid Dynamics Conference. San Antonio, Texas, USA, AIAA 2009–3992.
[16] Cao, H., Wan, D.C., 2010. Application of OpenFOAM to simulate three-dimensional flows past a single and two tandem circular cylinders. In: Proceedings of the 20th International Offshore and Polar Engineering Conference. Beijing, China, ISOPE, vol. 3. pp. 702–709.
[17] Zhou, H., Cao, H., Wan, D.C., 2013. Numerical predictions of wave impacts on the supporting structures of Shanghai Donghai-Bridge offshore wind turbines. In: Proceedings of the 23rd International Offshore and Polar Engineering Conference. Anchorage, Alaska, USA, ISOPE, vol. 1. pp. 216–224.
[18] Wang, J., Zou, L., Wan, D.C., 2017. CFD simulations of free running ship under course keeping control. Ocean Eng. 141, 450–464.
[19] F.R. Menter, Two-equation eddy-viscosity turbulence models for engineering applications, AIAA J. 32 (1994) 1598–1605.
[20] Sun, H., Kim, E. S., Nowakowski, G., Mauer, E., & Bernitsas, M. M. (2016). Effect of mass-ratio, damping, and stiffness on optimal hydrokinetic energy conversion of a single, rough cylinder in flow induced motions. Renewable Energy, 99, 936-959.
[21] Zhao, W.W., Zou, L., WAN, D.C., Hu, Z.Q, Numerical investigation of vortex-induced motions of a paired-column semi-submersible in currents. Ocean Engineering 2018(164), 272–283.
[22] Ye, H.X, Wan, D.C., Benchmark computations for flow around a stationary cylinder with high Reynolds numbers by RANS-overset grid approach. Applied Ocean Research 65(2017), 315-326
[23] H. Sun, E.S. Kim, P.M. Bernitsas, M.M. Bernitsas, Virtual spring damping system for flow-induced motion experiments, J. Offsh. Mech. Arct. Eng. 137 (6) (2015) 061801.

[24] Williamson, C.H.K. Sinusoidal flow relative to circle cylinders. J. Fluid Mech. Vol. 155, p. 141-174.
[25] Sarpkaya, T. Force on a circular cylinder in viscous oscillatory flow at low Keulegan-Carpenter number. J. Fluid Mech., 1986(a)165: 61-71
[26] Honji, H. Streaked flow around an oscillating circular cylinder. J. Fluid Mech., 1981(107): 509-520